Published in final edited form as:
Mol Pharm. 2009 ; 6(5): 1343–1352. doi:10.1021/mp900022m.

Flexible Filaments for *in vivo* Imaging and Delivery:

Persistent Circulation of Filomicelles Opens the Dosage Window for Sustained Tumor Shrinkage

David A. Christian[1], **Shenshen Cai**[1], **Olga B. Garbuzenko**[2], **Takamasa Harada**[1], **Allison L. Zajac**[1], **Tamara Minko**[2], and **Dennis E. Discher**[1,*]

[1]Department of Chemical and Biomolecular Engineering, University of Pennsylvania Philadelphia, PA 19104

[2]Department of Pharmaceutics, Rutgers, The State University of New Jersey, Piscataway, NJ 08854

Abstract

Shape effects of synthetic carriers are largely unexplored *in vivo*, although recent findings suggest that flexible filaments can persist in the circulation even if microns in length. Here, to better assess biodistribution, a near infrared fluorophore (NIRF) was incorporated into such block copolymer 'filomicelles', and both *in vivo* and *ex vivo* imaging show that the majority of these worm-like micelles remain in the circulation for at least a day after intravenous injection. NIRF imaging further suggests that filomicelles convect into a tumor and some fragments can penetrate into the tumor stroma. To assess a functional effect, the hydrophobic drug paclitaxel (tax) was loaded into both filomicelles and sonication-generated spherical micelles of the same copolymer. Intravenous injection of tax-loaded filomicelles nearly doubles the maximum tolerated dose of tax in normal mice compared to tax-loaded spherical micelles. In tumor-bearing mice, the higher dose of tax produces greater and more sustained tumor shrinkage and tumor cell apoptosis. These results thus begin to address mechanisms for how non-spherical carriers deliver both imaging agents and anti-cancer therapeutics to solid tumors.

Introduction

Carriers designed for imaging or drug delivery have almost always been spherical in shape with radii smaller than about 500 nm. Large particles tend to rapidly lodge in capillary beds and be cleared from circulation. The effects of carrier shape have been understudied, but have gained recent attention with both *in vitro* studies of cell uptake [1-4] and initial studies of *in vivo* drug delivery using filamentous micelles assembled from amphiphilic block copolymers.[3] Remarkably, flexible 'filomicelles' up to 8-μm long are not rapidly cleared and instead appear to circulate longer than spherical nano-assemblies composed of very similar PEG-based diblock copolymers.[3] Polymer-based cylinders of μm-diameter,[2] as well as our nm-diameter filomicelles,[3] frustrate clearance processes such as phagocytosis *in vitro*. Such findings suggest a potential explanation for persistent convection of filomicelles past the mononuclear phagocytic system (MPS) of the liver and spleen — which generally clears circulating nanoparticles within hours (Fig. 1 - left). While initial studies have indicated that circulating filomicelles can deliver drugs to tumors,[3] pharmacokinetic mechanisms have remained unclear. The primary goal of this study was to visualize *in vivo* filomicelle biodistribution, and secondarily to compare filomicelles directly to spherical micelles in drug dosage limits and anti-cancer efficacy.

*Corresponding author: discher@seas.upenn.edu, Phone: 215 898-4809; fax: 215-573-2093.

For real-time tracking of biodistribution *in vivo* and imaging of organ accumulation, drug carriers loaded with near infrared fluorophores (NIRFs) are of particular utility. NIRFs have the distinct advantage of exciting and emitting in the portion of the light spectra minimally absorbed by tissue.[5] Therefore, drug carriers loaded with NIRFs can be tracked in live animals using whole body scans that are both rapid and inexpensive compared to other imaging modalities.[6] Recent work has shown that the thick hydrophobic membrane core of polymer vesicles (polymersomes) can be loaded with hydrophobic porphyrin-based NIRFs for *in vivo* imaging.[7, 8] For the filomicelles in this study, an amphiphilic NIRF similar in structure to other 'cell tracking' dyes used *in vivo* 9 was integrated at low weight percent into filomicelles. NIRF-labeled filomicelles emitted sufficient signal to image not only carrier dispersion within a tumor-bearing mouse, but also NIRF-labeled micelles within isolated tissues and blood.

Hydrophobic drugs such as the anticancer drug paclitaxel are also readily loaded into the filomicelles.[3, 10-12] Paclitaxel (tax) is routinely used in clinical treatments of many types of solid tumors as it induces cell death through the stabilization of microtubules.[13] However, the low solubility and severe side effects of tax to normal organs [14] limit high dose administration and require the use of a solubilizing agent. Chremophor® EL is the most common clinical solubilizing agent, but this emulsifier has its own dose-limiting side effect, namely cardiotoxicity and nephrotoxicity *in vivo*.[15-17] Previous *in vitro* studies with human lung cancer derived A549 cells compared the cytoxicity of Chremophor® and polymer micelles composed of degradable PEG-poly(ε-caprolactone) (OCL3); the polymer micelles used here are 5-fold more cytotoxic in delivering tax and also far less toxic as empty carriers.[10] Compared to spherical micelles made with the same block copolymer, filomicelles also provide a 2-fold increase in tax dose-loading.[10] Initial *in vivo* studies demonstrated that tax-loaded filomicelles shrink tumors.[3] These results motivated the drug delivery studies which show filomicelles increase the maximum tolerated dose (MTD) of tax relative to spherical micelles. Additionally, we show that filomicelles tend to minimize off-target delivery and maximize delivery to a tumor. The results lend insight into whether filomicelles, their fragments, and/or the delivered drug tax can penetrate into the tumor stroma *via* enhanced permeation and retention (EPR) that is typical of tumors when compared to other organs (Fig. 1 - right).

2. Materials and Methods

2.1 Materials

Degradable diblock copolymers composed of poly(ethylene oxide)-*b*-poly(ε-caprolactone), namely PEO_{110}-PCL_{58} (denoted OCL3), PEO_{45}-PCL_{75} (OCL 2-8.5), and also PCL_{44} were synthesized by ring-opening polymerization or purchased from Polymersource, Inc. (Dorval, Canada). The inert diblock copolymer poly (ethylene oxide)-poly(ethylethylene) (PEO_{42}-PEE_{35}, denoted OEX) was obtained from Dr. Frank S. Bates (University of Minnesota). Paclitaxel (tax), docetaxel, and Dulbecco's phosphate-buffered saline (PBS) were from Sigma (St. Louis, MO). Ncr nude mice (female, ~5 weeks, 20 g) were purchased from Taconic Farms, Inc. (Germantown, NY). Cell death detection ELISA^{plus} kit was purchased from Roche (Indianapolis, IN). Human lung carcinoma cells A549 were obtained from ATCC (Manassas, VA). F12 Ham media was purchased from Mediatech, Inc. (Herndon, VA). All organic solvents were analytical grade from Fisher Scientific. The near-infrared lipophilic dye, DiR, as well as Hoescht 33342, and rhodamine-maleimide were purchased from Invitrogen, Inc.

2.2 Formation of filomicelles and spherical micelles

Inert, NIRF-labeled OEX filomicelles were formed by standard film rehydration techniques. Filomicelles were labeled with the lipophilic, NIR fluorophore DiR, by dissolving DiR in methanol and adding it to the chloroform solution containing dissolved polymer. The chloroform/methanol solution was then dried off by nitrogen purge and subsequent vacuum

for 24 h. These fluorophore-labeled polymer films were then hydrated at 60°C with deionized water. Concentrated filomicelle solutions (5 mg/mL) were hydrated 24 h at 60°C without stirring, followed by an additional 24 h at 60°C with gentle stirring. OEX filomicelles were filtered for large aggregates by diluting the concentrated solution 20X and extruding through 10 μm, 1 μm, and 0.4 μm pore size filters at low pressures. Filomicelles were then concentrated using Amicon Ultra Centrifugal Devices (5K and 10K NMWL). To remove any excess DiR, filomicelles were dialyzed (10K MWCO) against deionized water for 24 h. A final buffer exchange was performed by dialyzing into PBS for at least 6 h. Visual confirmation of DiR-labeled filomicelles was done by epifluorescence microscopy (Olympus IX71).

OCL filomicelles and spherical micelles were formed by a solvent evaporation method as previously described.[10] Briefly, an OCL stock solution in chloroform was mixed with deionized water and the mixture was stirred at room temperature until chloroform was completely evaporated. OCL3 spherical micelles were obtained by sonicating the OCL3 filomicelles using a Fisher 60 Sonic Dismembrator. OCL (2-8.5) filomicelles were fragmented by repeated heating and cooling cycles. The size distribution of these spherical micelles and fragmented filomicelles were measured by dynamic light scattering.

2.3 Tax loading of OCL micelles

A tax stock solution in methanol was added into the micelle solution to obtain desired spiked tax/polymer ratios that were constant between filomicelles and spherical micelles. The mixture was stirred at 25°C for 20 min, dialysed against PBS for 2 h, and filtered by extrusion to remove any tax aggregates.

2.4 Biodistribution with NIRF labeled filomicelles

Tumor xenografts grew following subcutaneous injection of 10^7 A549 lung cancer cells expressing luciferase. Tumors were allowed to grow for 4 weeks, before NIRF-labeled filomicelles were injected into the tail veins of tumor-bearing nude mice. After 24 h, the xenografted mice were injected with luciferin 10 minutes before imaging, and were then imaged for luminescence and also NIR fluorescence using a Xenogen IVIS Lumina. The mice were then sacrificed and whole blood, liver, spleen, lungs, kidneys, heart, brain, and tumor were collected. The whole blood was then centrifuged and plasma collected.

Whole organs were imaged on the Licor Odyssey using the 800 nm excitation laser. To correct for loss of fluorescence intensity due to organ thickness and optical properties, three fresh organs of each type were cut into progressively thinner sections using standard dissection tools. These organs were imaged after each iteration until the sum of section intensities converged. The ratio in the fluorescence integrated intensity between the whole and iteratively sectioned organs was calculated as the organ correction factor and applied to all other measured intensities for whole organs. The intensity of the plasma was calculated by serially diluting the plasma in PBS and imaging in a 96 well plate on the Licor. The slope of the linear dilution curve provided an accurate measurement of the fluorescence intensity per 100 μL of plasma. Filomicelles remaining in the blood were imaged by epifluorescence at 60X after a ten-fold dilution of the plasma in PBS.

2.5 Cryo sectioning and immunostaining of A549 tumor xenografts

Immediately after Licor whole organ imaging, excised tumors were suspended in OCT medium and frozen in liquid nitrogen. Frozen tumor tissues were sectioned on a Leica cryostat microtome (10 μm sections). A glass grid with numbered 500 μm squares (Electron Microscopy Sciences) was super-glued to the bottom of the slides under the tissue for reference. Phosphate buffered saline (PBS) with 1 μg/ml Hoechst trichloride trihydrate was added to rehydrate the tissue and visualize the nuclei. Epifluorescence microscopy at 20X magnification was used to

take 5-7 images of the NIR signal, nuclei, and grid of the unfixed samples. After imaging, samples were fixed in 3.7% Formaldehyde in PBS for 10 min, washed with PBS, permeabilized with 0.5% Triton-X100 for 10min, and washed again with PBS. Samples were blocked with 10% cow serum for 30min and stained with the human-specific antibody Lamin A/C (Santa Cruz Biotechnology clone 636) at 1:100 in blocking solution, washed in PBS, and stained at 1:300 with an AlexaFlour-488 congujated secondary antibody for 1 h (Molecular Probes). After final washing, samples were mounted with GelMount (Biomeda) and the same regions were reimaged using the grid as reference.

2.6 Maximum Tolerated Dose (MTD) determination

A concentration series of tax in OCL3 micelles [10, 18] was prepared in PBS at 0.5, 1, and 2 mg/mL for spherical micelles (corresponding to 5, 10, and 20 mg/kg for 20 g mice with 0.2 mL injection per animal) and 0.5, 1, 2 and 3 mg/mL for filomicelles (corresponding to 5, 10, 20, and 30 mg/kg for 20 g mice with 0.2 mL injection per animal). The same concentrations of empty OCL3 micelles were also prepared. Nrc nude mice were weighed followed by a single tail vein injection of both empty OCL3 micelles and tax-loaded micelles in different concentrations at 0.2 mL per mouse. After 24 h, the mice were weighed again. The maximum tolerated dose was determined as the dose that caused the mouse body weight loss <10%.[19]

2.7 Tumor shrinkage studies

Human lung carcinoma cell line, A549, was injected subcutaneously at 10^7 per mouse. After about 3 weeks, the tumor-bearing mice were injected with tax-loaded OCL3 micelles at MTD of the corresponding morphology, as well as free tax at MTD (1 mg/kg),[19] and PBS saline alone. The same injections were repeated after 3, 7, 10, 14, 17, 21 days. Tumor area (A) was monitored 24 h after each injection by measuring two orthogonal dimensions as $A = [(L_1 \times L_2) / 2]$ for each treatment group.[19] The body weight of the mice was also monitored throughout the experiment.

2.8 Cell apoptosis in tumor and non tumor organs

A DNA-based photometric enzyme immunoassay system (Cell Death Detection ELISA) was employed to evaluate the cell apoptosis within organs. The mice subjected to treatments above were sacrificed after 22 days and their organs, including liver, kidney, spleen, heart, lung and tumor, were removed. Those organs were weighed and homogenized by Dounce Homogenizer (Belco Glass, Vineland, NJ). The supernatant after centrifugation was then used to determine the specific enrichment of nucleosomes released into the cytoplasma due to the death of the cells, following the manual supplied with the ELISA kit. The cell apoptosis index was calculated as: Enrichment factor of tax treatment animal groups / Enrichment factor of untreated animal groups. The cell apoptosis index for the untreated groups was designated 1.

2.9 Biodistribution studies for tax loaded OCL3 micelles

The distribution for tax in mice was determined by an HPLC method. Briefly, at 24 h after a single tail vein injection of tax-loaded OCL3 micelles and free tax, the tumor-bearing mice were sacrificed and their liver, kidney, spleen, heart, lung and tumor were removed. Those organs were weighed, and homogenized in 1-2 ml 1:1 acetonitrile (ACN):H_2O with addition of 50 μl of 10 μg/ml docetaxel as the internal standard. The homogenate was then mixed with 5 ml ethyl acetate for 24 h. After centrifugation at 6000 rpm, 4 °C for 10 min, the supernatant was transferred to a new vial, dried under N_2 stream, and reconstituted with 200 μl ACN. The solution was filtered through 0.45 μm poly (tetrafluoroethylene) (PTFE) filter and then subjected to HPLC with the same method as described previously.[10]

2.10 Uptake of OCL micelles by A549 cells in vitro

Fluorescent OCL filomicelles that contain 5 mol% rhodamine-labeled PCL were subjected to fragmentation. A PCL-SH block was covalently labeled with rhodamine-maleimide by standard Michael reaction. 5×10^3 A549 cells were transferred to Matek dishes (35 mm) 24 h prior to the addition of micelles. After addition of fresh media (Ham's F12), micelles were added at a polymer concentration of 50 μM and incubated for 24 h. After incubation, the supernatant was removed and saved, and cells were washed with PBS 3 times. Cell nuclei were then stained with Hoescht 33342 dye *without fixation*. Cells were imaged by epifluorescence microscopy for micelle uptake and nuclear localization, and also imaged by differential interference contrast microscopy to identify cell boundaries.

3. Results

3.1 — Imaging NIRF labeled filomicelles in tumor bearing mice

Filomicelles have been shown to circulate for days *in vivo*, and, more importantly, can shrink tumors when loaded with the hydrophobic anti-cancer drug paclitaxel.[3] However, where these carriers accumulate in tumor-bearing mice and how drug is delivered to the tumor has not yet been elucidated. To better assess the effects of shape on carrier biodistribution, inert OEX filomicelles were loaded with the NIR fluorophore, DiR. OEX filomicelles might fragment mechanically but will not degrade hydrolytically [18]; as such they are not expected to release the dye *in vivo* 3 and are therefore useful to determine carrier localization in the tumor architecture.

NIRF-labeled OEX filomicelles were injected into the tail vein of luciferase-positive A549 tumor-bearing mice. Whole body imaging of these mice was conducted 24 h after tail vein injection of filomicelles and 10 min after luciferin administration, showing luminescent tumors (Fig. 2A) and relatively uniform NIR fluorescence throughout filomicelle-injected mice (Fig. 2B); negative control mice that were not injected with NIRFs showed no significant NIR fluorescence (not shown). Rather than concentrating in select organs or tissues, filomicelles appeared dispersed by continued circulation, consistent with past reports based only on imaging of blood samples.[3]

Organs and whole blood were collected from mice that were sacrificed at 24 h, and NIR fluorescence images of whole organs and serially diluted blood plasma were acquired to determine integrated fluorescence intensity. Compared to negative controls, which showed very little NIR fluorescence, filomicelles accumulate in multiple organs, including excised tumors. Low resolution fluorescence imaging of the excised tumor shows a significant accumulation of NIRF-labeled filomicelles in the tissue (Fig. 2C). Brain tissue is comparatively transparent, and its well-organized vasculature — separated by a relatively impermeable blood-brain barrier — is particularly clear in both low resolution fluorescence images (Fig. 2D) and also in high resolution images (Fig. 2E). NIRF-labeled filomicelles thus appear to persist in the circulation when directly examined.

To quantify the biodistribution of filomicelles in the tumor-bearing mice, the NIR fluorescence intensities of each tissue were measured, integrated, and experimentally corrected for thickness and optical absorbance (see Methods 2.4). Blood was bright, and high resolution epifluorescence imaging of plasma shows that the fluorescence intensity is due to NIRF-labeled filomicelles that persist in blood for at least 24 h (Fig. 3, inset). The total blood contribution to the intensity of each tissue was calculated using (*i*) previous estimates of the blood volume fraction for each tissue type,[20, 21] (*ii*) the measured tissue weight (assumed organ density ~ 1 g/mL), and (*iii*) the NIR intensity measured for blood. These corrected organ fluorescence estimates were then summed and normalized for the total fluorescence intensity measured per

mouse to reveal the relative amount of NIRF-labeled filomicelles within the stroma of each tissue type (Fig. 3). As expected, uptake was highest in the MPS organs (livers and spleens) and lowest in the brains where filomicelles would not be expected to cross the blood-brain barrier. Tumor intensities (I) were significantly higher than brain intensities ($p < 0.004$) as well as tumor intensities (I_0) from mice that received no NIRF-labeled filomicelles ($I/I_0 = 141$; $p < 0.004$), which clearly indicates accumulation of filomicelles within the tumor.

3.2 — Imaging NIRF labeled filomicelles in tumor sections

High resolution epifluorescence microscopy of tumor cryo-sections revealed the accumulation of NIRF-labeled filomicelles in distinct regions of the tissue (Fig. 4A). To try to determine more specifically where NIRF-labeled filomicelles localized within the tumor architecture, frozen tissue sections were stained to specifically identify human A549 cancer cells using a monoclonal anti-human Lamin A/C antibody. Lamin A/C is a structural protein intrinsic to the nuclear membrane of most somatic cells, including A549 cells.[22] Hoescht stains all cell nuclei, whereas the Lamin A/C antibody is specific for the xenografted tumor cells (Fig. 4B). This specificity allows for identification of tumor stroma distinct from the tumor vasculature that is composed of only mouse cell types.

Lamin A/C and Hoescht colocalize throughout most of the stroma of the sectioned tumor, which appears disorganized in architecture (Fig. 4B); focal regions that are negative for Lamin A/C are mouse-derived cells and likely part of the tumor vasculature. NIR fluorescence invariably localizes in these ‘mouse’ regions as well (Fig. 4C), which is consistent with filomicelles being predominantly in the vasculature. However, unlike brain (Fig. 2D), a fraction of NIR fluorescence permeates perhaps a few cell layers into the human xenograft (i.e. green Lamin A/C positive). These images thus show that — on a time scale (24 h) at which an anticancer drug is shown below to shrink a tumor significantly — filomicelles and/or their fragments will permeate the tumor stroma even though most of the carrier is still in circulation.

3.3 Almost two fold higher MTD for tax in OCL3 filomicelles compared to OCL3 spheres

The tumor localization of NIRF-labeled filomicelles (or their fragments) motivated further study of the functional delivery of a drug (specifically paclitaxel or ‘tax’). Additionally, a more direct assessment of shape effects was conducted by comparing filomicelles to what are essentially spherical micelles obtained by extensive sonication-induced fragmentation of the filomicelles.[10] First, the maximum tolerated dose (MTD) for each tax carrier was determined using the common benchmark of 10% loss of body weight at 24 h. No significant weight loss was observed with the drug-free polymeric carriers across the entire range of polymer concentrations tested (Fig. S1); and when loaded with tax, the tax-Filomicelles appeared significantly less toxic than the tax-Spheres at every concentration tested (Fig. 5A). In terms of the MTD, mice injected with tax-loaded OCL3 filomicelles showed an enhanced tax tolerance ($MTD_{Fil} \approx 18$ mg/kg) compared to mice injected with tax-loaded OCL3 spherical micelles ($MTD_{Sph} \approx 10$ mg/kg); note also that free drug is known to have a far lower $MTD_{tax} \approx 1$ mg/kg. The considerable increase in the MTD when drug is delivered with filomicelles allows for a higher dosage to be administered into tumor-bearing mice and portends an improved therapeutic effect as examined below.

3.4 The enhanced MTD with filomicelles produces a better tumor shrinkage effect

The effect of the different tax carriers on tumor growth was examined with the xenografted mice injected twice a week for three weeks — a relatively standard clinical course of chemotherapy. To reduce the potential for tax-induced side effects, animals were injected at tax concentrations just below the MTD: 16 mg/kg of tax-filomicelles and 8 mg/kg of tax-spherical micelles. Free tax diluted in PBS was injected at MTD_{tax} (1 mg/kg). While all of these tax formulations showed at least some suppression of tumor growth (Fig. 5B, upper

panel), all tumor-bearing mice appeared otherwise similar in overall health with similar weight gains and no significant weight differences between groups (Fig. 5B, lower panel). Note that tumors are not expected to contribute to differences because even the largest, untreated tumor area at 3 weeks was only 0.4 cm^2 and thus corresponds to an approximate weight gain of only 0.2 g for a ~20 g mouse.

Compared to the control group in which only PBS was injected, tax administration in any form consistently and significantly inhibited tumor growth when measured just prior to the second injection on day 3. At this timepoint, tumor sizes were significantly different ($p < 0.05$) in the order: (MTD_{tax})-treated tumors > (MTD_{Sph})-treated tumors > (MTD_{Fil})-treated tumors. This trend was not only maintained throughout the 22 day treatment, but by the end the 22 day treatment only the (MTD_{Fil})-treated tumors maintained the reduced tumor size and showed no increase in size, appearing substantially better than any other treatment group.

For further comparison of the effect of carrier shape alone, tax-filomicelles were also injected at MTD_{Sph}. This decrease in tax concentration resulted in nearly identical tumor shrinkage as seen with spherical micelles at MTD_{Sph} (Fig. 6A), which simply highlights the critical importance of drug dosage. Further measurements below will nonetheless show that tax-filomicelles even at MTD_{Sph} minimize side-effects, consistent with opening the dosage window: $MTD_{Fil} > MTD_{Sph}$.

3.5 Filomicelles improve the specificity of tumor cytotoxicity

Cell death is important to evaluate within key organs as well as the tumors. Apoptosis within a tumor should correlate with antitumor effects, whereas apoptosis in non-tumor organs should relate to dose-limiting side effects of the drug (i.e. MTD). Measurements of apoptosis within the six tested major organs (liver, kidney, spleen, heart, lung, and tumor) show as expected that mice injected with PBS or polymeric micelles alone have the same low, baseline level of apoptotic cells (Fig. 6A). In contrast, all formulations of tax showed a significant level of apoptosis in all organs, demonstrating broad cytotoxicity of the drug.

While free tax did not exhibit good tumor specificity, with less than 2-fold difference in apoptosis between the tumors and any of the non-tumor organs, delivery of tax with all of the OCL3 micelles showed greater apoptosis in the tumor without greatly increasing apoptosis in the non-tumor organs compared to free drug (Fig. 6A). Filomicelles and spherical micelles loaded with the same tax at 8 mg/kg showed no significant difference between tumor apoptosis, but the apoptosis in non-tumor organs was 15-30% *lower with filomicelles* than with spherical micelles. When the tax dose was doubled to 16 mg/kg with filomicelles, tumor apoptosis showed a proportional increase (2-fold) whereas apoptosis in non-tumor organs showed only a modest increase (30-40%), which is consistent with filomicelles shifting the effective activity and biodistribution of drug away from these major non-tumor organs.

The ratios of cell apoptosis in the tumor versus non-tumor organs is plotted and tabulated to clarify the differences above (Fig. 6B and Table 1). Compared to spherical micelles, filomicelles clearly increase the tumor-selective cytotoxicity of tax by about 30-60% at a tax dose of either 8 or 16 mg/kg. This enhancement in tumor selectivity by filomicelles or filomicelle fragments is especially evident in the heart and lungs (non-MPS organs), which could result from the increase in the effective size compared to spherical micelles.[10] This is consistent with the EPR effect where the tight vasculature of the non-tumor organs inhibits permeation of larger objects, while the leaky vasculature of the tumor is equally permissive for both carriers (Fig. 1).

3.6 Tax delivered by filomicelles also accumulates more in the tumor

To understand apoptosis in relation to injected drug, the distribution of tax *in vivo* was measured. Tumor xenografted mice were sacrificed 24 h after a single intravenous dose of the various forms of tax. The biodistribution of tax — as measured after extraction by HPLC — confirmed that tax delivered by polymeric micelles accumulates in the tumors more so than tax injected as free drug (Fig. 7A). It was verified that tax in OCL3 micelles was stable and the gradual release kinetics were similar between micelle shapes in PBS and in serum (Fig. S2). Moreover, at 24 h, filomicelles and spherical micelles at the same tax dose (8 mg/kg) show that filomicelles enhance the tumor / organ selectivity by about a factor of 2. The 16 mg/kg dose of tax-filomicelle (i.e. MTD_{Fil}) is shown to increase the amount of drug in all organs except kidney. This overall biodistribution profile is consistent with the higher tumor-specific apoptosis associated with filomicelles.

Accumulation of tax appears to correlate linearly with apoptosis in tumors for all carriers ($R^2 = 0.98$) and also with apoptosis in the MPS organs, the liver and spleen (Fig. 7B). Tax concentrations are therefore expected to be in the range of known cytotoxic doses, which for free tax in cultures of A549 cells is $IC_{50} = 0.32$ μM.[10] Apparent concentrations of tax in organs were estimated from the molecular weight of tax (850 g/mol) and by approximating tissue density as 1 g/mL. Injection of free tax, which yields the lowest levels of drug, delivers an organ-average ~1 μM drug concentration into liver, spleen, and tumor, and all of these organs showed similar levels of apoptosis just above baseline levels. Based on this analysis, all of the micelle carrier systems deliver tax in the cytotoxic range. Furthermore, because the dose-response *in vivo* appears linear — rather than saturating — for all organs, no therapeutic efficacy of tax is lost when micellar carriers deliver high concentrations of tax to tumors.

3.7 in vitro study of uptake of filomicelles by A549 cells

Motivated by all of the *in vivo* studies above, we performed an *in vitro* study to assess whether filomicelle fragments can be taken up by the A549 cancer cells. Past studies had suggested that long filomicelles are unlikely to be internalized and also that filomicelles fragment in the circulation, but past studies had not clearly addressed whether fragments can be taken up by these cells in culture. Furthermore, the cytotoxicity of tax results from the stabilization of microtubules that prevents cellular processes such as mitosis, and therefore requires tax to be delivered to the cytosol. It is therefore important to not only understand where filomicelles accumulate in the tumor architecture (Fig. 4), but also the way in which their shape might determine how they deliver tax intracellularly within the tumor. OCL filomicelles (OCL 2-8.5) labeled with a rhodamine-labeled PCL block were fragmented and then incubated with A549 cells in culture for 24 h. Epifluorescence microscopy after 24 h clearly indicated that fragmented filomicelles — with length approximated by fluorescence intensity analysis (Fig. S3) — could indeed be internalized with classic perinuclear localization (Fig. 8).

4. Discussion

While chemotherapeutics such as tax kill tumor cells, these drugs also permeate many non-tumor organs where their cytotoxicity limits the dose that can be administered to patients (or model organisms such as mice). Filomicelles visualized here by NIRF-labeling are shown to delay the rapid clearance by the MPS (liver and spleen) that is typical of nanoparticles; NIRF-labeled filomicelles persist in the blood circulation for at least 24 h (Fig. 2B, 3). Filomicelles might therefore be expected to minimize the accumulation of cytotoxic drugs such as tax in healthy organs. Based on comparisons here with spherical micelles composed of the same copolymer, the novel morphology of filomicelles indeed increases the MTD of tax, allowing higher doses to be administered (Fig. 5).

Consistent with a higher MTD for tax-loaded filomicelles compared to tax-loaded spherical micelles, a decrease in tax accumulation in major organs relative to more permeable tumors was measured and found consistent with trends in apoptosis (Fig. 6,7). Shape-dependent decreases in apoptosis were not limited to the liver and spleen but were also observed in the heart and lungs (Fig. 6B, 7A). The results thus indicate that the tumor selectivity of filomicelles compared to spherical micelles is not only dependent on the ability of filomicelles to evade clearance by the immune system, but also on the ability of micelles to permeate into different tissues as a function of shape. Moreover, while filomicelles seem less likely to permeate into healthy tissue compared to spherical micelles, the leaky vasculature of the tumor that defines the Enhanced Permeation and Retention (EPR) effect might be permissive for longer filomicelles or filomicelle fragments (Fig. 4). Imaging of tumor sections is currently unable to reveal the length of these filomicelles to determine whether intact, μm-long filomicelles or fragmented filomicelles were the morphology responsible for the accumulation of the NIR fluorescence. A likely model is that filomicelles circulate and shear apart into fragments that are too large to accumulate in healthy tissue (Fig. 2D,E) but are small enough to accumulate in the tumor (Fig. 2C, 4) and perhaps tumor cells (Fig. 8). If longer filomicelles could also enter the tumor stroma, they are likely to release tax outside tumor cells as the OCL polymer hydrolytically degrades because long filomicelles cannot be taken up into cultured cells.[3] Such a delivery mechanism could nonetheless be effective as tax readily permeates cell membranes.

'Effectiveness' can be made more quantitative by fitting a simple model [23] to the graphs of tumor size *versus* time in Fig. 5B. The model is just a sum of exponential phase tumor growth and drug-induced tumor shrinkage, and Table 2 gives the three fitting parameters for the tumor area function below:

$$(\text{Tumor Area}) = A \quad exp\left(t/\tau_{\text{growth}}\right) + B \quad exp\left(-t/\tau_{\text{shrink}}\right),$$

noting that A and B are prefactors, t is time in weeks, τ_{growth} and τ_{shrink} are the fitting constants for tumor growth and tumor shrinkage, and $B = (Tumor\ Area)_o - A$ with $(Tumor\ Area)_o \approx 0.17\ cm^2$. In the absence of injected tax (Controls), the growth phase fits very well to a single exponential ($R^2 = 0.99$) with a time-constant of $\tau_{\text{growth}} = 3.5$ weeks, indicating that there is no tumor shrinkage. With free tax, a very good fit is obtained with the same τ_{growth} and a somewhat faster $\tau_{\text{shrink}} = 1.1$ weeks. With spherical micelles, in contrast, the growth phase is slowed from 3.5 weeks to more than 2 months, whereas with filomicelles, growth is slowed to greater than 1 year. For both micelle morphologies, tumor shrinkage times are a relatively rapid 2-3 days. The fitting results thus indicate that while tax-induced shrinkage is rapid and tax-micelles do generally slow tumor growth, tax-filomicelles can slow tumor growth more than 6-fold compared to spherical micelles. Inhibition of tumor growth by tax-filomicelles lasts up to about a year, which is essentially sustained shrinkage.

While tax-filomicelles shrink the tumor and suppress growth, a 'lump' remains throughout the 3 week period. To analyze this quantitatively within the collective trend, a plot of the relative shrinkage of the estimated tumor volume (calculated from the tumor area by assuming the tumor is a sphere) *versus* the relative tumor apoptosis at day 22 was fit to a 'growth law' [24] type of expression where *a, b*, and *k* are fitting constants (Fig. 9):

$$(\text{Tumor shrinkage}) = b - a \quad exp\left[-k \times (\text{Cell death})\right]$$

The fit proved excellent ($R^2 = 0.999$) and gave a maximum tumor shrinkage of 88.9% (= b). This maximum is below 100% and could be due to residual matrix and/or the development of drug-resistant tumor cells. Importantly, in mice treated with tax-filomicelles, the tumor shrinks

87%, which is essentially the same as the fitted maximum, *b*. Therefore, it seems plausible, based on the trends here, that tumors cannot be shrunk more than what is possible with tax-filomicelles loaded at the high drug dose (MTD_{FIL}) that is allowable by the distinctive and flexible filamentous shape of these carriers.

Supplementary Material

Refer to Web version on PubMed Central for supplementary material.

Acknowledgements

We would like to thank Dr. Natalie Christian for her technical support with the NIR imaging experiments. This study was supported by grants from NIH-NIBIB, NTI, and NSF-MRSEC.

References

1. Champion JA, Katare YK, Mitragotri S. Particle shape: A new design parameter for micro- and nanoscale drug delivery carriers. Journal of Controlled Release 2007;121:3–9. [PubMed: 17544538]
2. Champion JA, Mitragotri S. Role of target geometry in phagocytosis. Proceedings of the National Academy of Sciences of the United States of America 2006;103:4930–4934. [PubMed: 16549762]
3. Geng Y, Dalhaimer P, Cai SS, Tsai R, Tewari M, Minko T, Discher DE. Shape effects of filaments versus spherical particles in flow and drug delivery. Nature Nanotechnology 2007;2:249–255.
4. Gratton SEA, Ropp PA, Pohlhaus PD, Luft JC, Madden VJ, Napier ME, DeSimone JM. The effect of particle design on cellular internalization pathways. Proceedings of the National Academy of Sciences of the United States of America 2008;105:11613–11618. [PubMed: 18697944]
5. Weissleder R. A clearer vision for in vivo imaging. Nature Biotechnology 2001;19:316–317.
6. Willmann JK, van Bruggen N, Dinkelborg LM, Gambhir SS. Molecular imaging in drug development. Nature Reviews Drug Discovery 2008;7:591–607.
7. Christian NA, Milone MC, Ranka SS, Li GZ, Frail PR, Davis KP, Bates FS, Therien MJ, Ghoroghchian PP, June CH, Hammer DA. Tat-functionalized near-infrared emissive polymersomes for dendritic cell labeling. Bioconjugate Chemistry 2007;18:31–40. [PubMed: 17226955]
8. Ghoroghchian PP, Frail PR, Susumu K, Blessington D, Brannan AK, Bates FS, Chance B, Hammer DA, Therien MJ. Near-infrared-emissive polymersomes: Self-assembled soft matter for in vivo optical imaging. Proceedings of the National Academy of Sciences of the United States of America 2005;102:2922–2927. [PubMed: 15708979]
9. Kalchenko V, Shivtiel S, Malina V, Lapid K, Haramati S, Lapidot T, Brill A, Harmelin A. Use of lipophilic near-infrared dye in whole-body optical imaging of hematopoietic cell homing. Journal of Biomedical Optics 2006;11
10. Cai SS, Vijayan K, Cheng D, Lima EM, Discher DE. Micelles of Different Morphologies -Advantages of Worm-like Filomicelles of PEO-PCL in Paclitaxel Delivery. Pharm. Res 2007;24:2099–2109. [PubMed: 17564817]
11. Dalhaimer P, Engler AJ, Parthasarathy R, Discher DE. Targeted worm micelles. Biomacromolecules 2004;5:1714–1719. [PubMed: 15360279]
12. Geng Y, Discher DE. Visualization of degradable worm micelle breakdown in relation to drug release. Polymer 2006;47:2519–2525.
13. Kim TY, Kim DW, Chung JY, Shin SG, Kim SC, Heo DS, Kim NK, Bang YJ. Phase I and pharmacokinetic study of Genexol-PM, a cremophor-free, polymeric micelle-formulated paclitaxel, in patients with advanced malignancies. Clinical Cancer Research 2004;10:3708–3716. [PubMed: 15173077]
14. Gligorov J, Lotz JP. Preclinical pharmacology of the taxanes: Implications of the differences. Oncologist 2004;9:3–8. [PubMed: 15161985]
15. Fetterly GJ, Tamburlin JM, Straubinger RM. Paclitaxel pharmacodynamics: Application of a mechanism-based neutropenia model. Biopharmaceutics & Drug Disposition 2001;22:251–261.

16. Kim SC, Kim DW, Shim YH, Bang JS, Oh HS, Kim SW, Seo MH. In vivo evaluation of polymeric micellar paclitaxel formulation: toxicity and efficacy. Journal of Controlled Release 2001;72:191–202. [PubMed: 11389998]

17. Xie JW, Wang CH. Self-assembled biodegradable nanoparticles developed by direct dialysis for the delivery of paclitaxel. Pharmaceutical Research 2005;22:2079–2090. [PubMed: 16132339]

18. Geng Y, Discher DE. Hydrolytic degradation of poly(ethylene oxide)-block-polycaprolactone worm micelles. Journal of the American Chemical Society 2005;127:12780–12781. [PubMed: 16159254]

19. Ahmed F, Pakunlu RI, Brannan A, Bates F, Minko T, Discher DE. Biodegradable polymersomes loaded with both paclitaxel and doxorubicin permeate and shrink tumors, inducing apoptosis in proportion to accumulated drug. J Control Release. 2006

20. Alexandrakis G, Rannou FR, Chatziioannou AF. Tomographic bioluminescence imaging by use of a combined optical-PET (OPET) system: a computer simulation feasibility study. Physics in Medicine and Biology 2005;50:4225–4241. [PubMed: 16177541]

21. Brown RP, Delp MD, Lindstedt SL, Rhomberg LR, Beliles RP. Physiological parameter values for physiologically based pharmacokinetic models. Toxicology and Industrial Health 1997;13:407–484. [PubMed: 9249929]

22. Pajerowski JD, Dahl KN, Zhong FL, Sammak PJ, Discher DE. Physical plasticity of the nucleus in stem cell differentiation. Proceedings of the National Academy of Sciences of the United States of America 2007;104:15619–15624. [PubMed: 17893336]

23. Simeoni M, Magni P, Cammia C, De Nicolao G, Croci V, Pesenti E, Germani M, Poggesi I, Rocchetti M. Predictive pharmacokinetic-pharmacodynamic modeling of tumor growth kinetics in xenograft models after administration of anticancer agents. Cancer Research 2004;64:1094–1101. [PubMed: 14871843]

24. Guiot C, Degiorgis PG, Delsanto PP, Gabriele P, Deisboeck TS. Does tumor growth follow a "universal law"? Journal of Theoretical Biology 2003;225:147–151. [PubMed: 14575649]

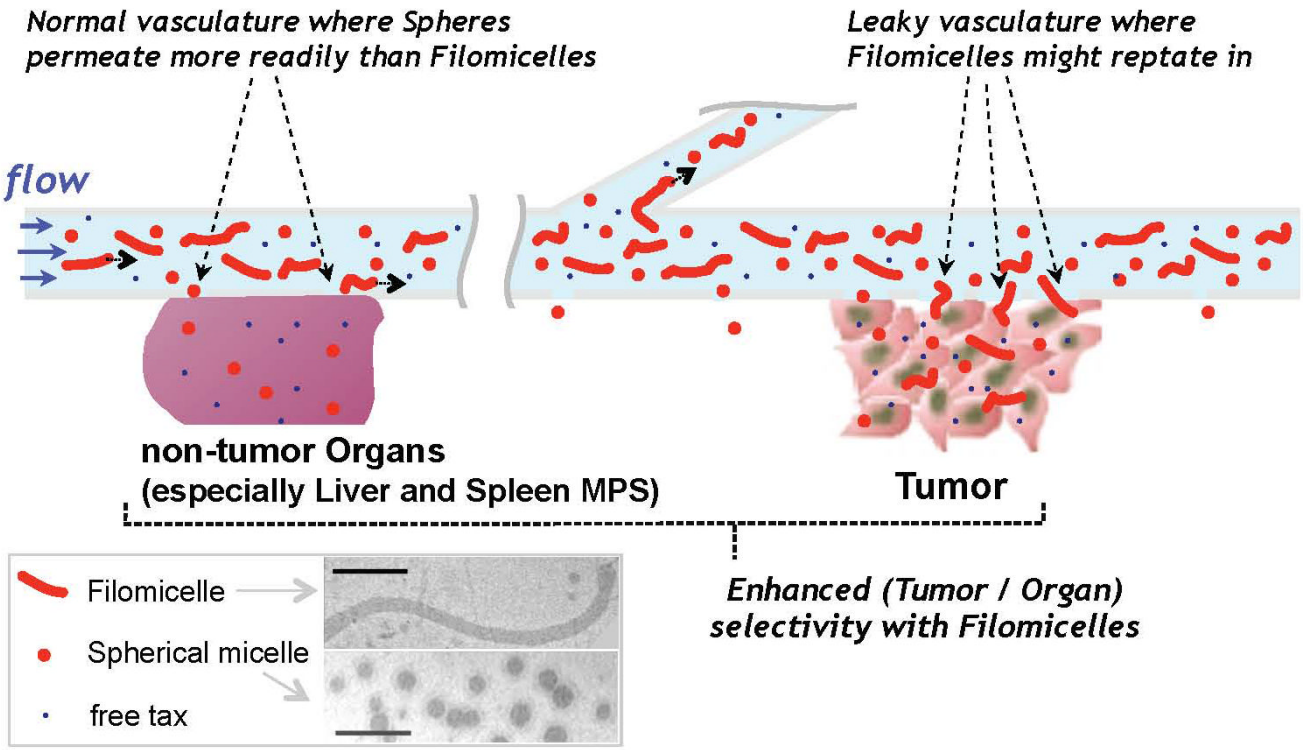

Figure 1. Sketch of drug delivery by spherical micelles and filomicelles

Filomicelles are more likely to accumulate preferentially in the tumor over other non-tumor organs due to the tumor-featured enhanced permeation and retention (EPR). Inset: Cryo-TEM images of OCL spherical micelles and filomicelles, scalebars 100 nm.

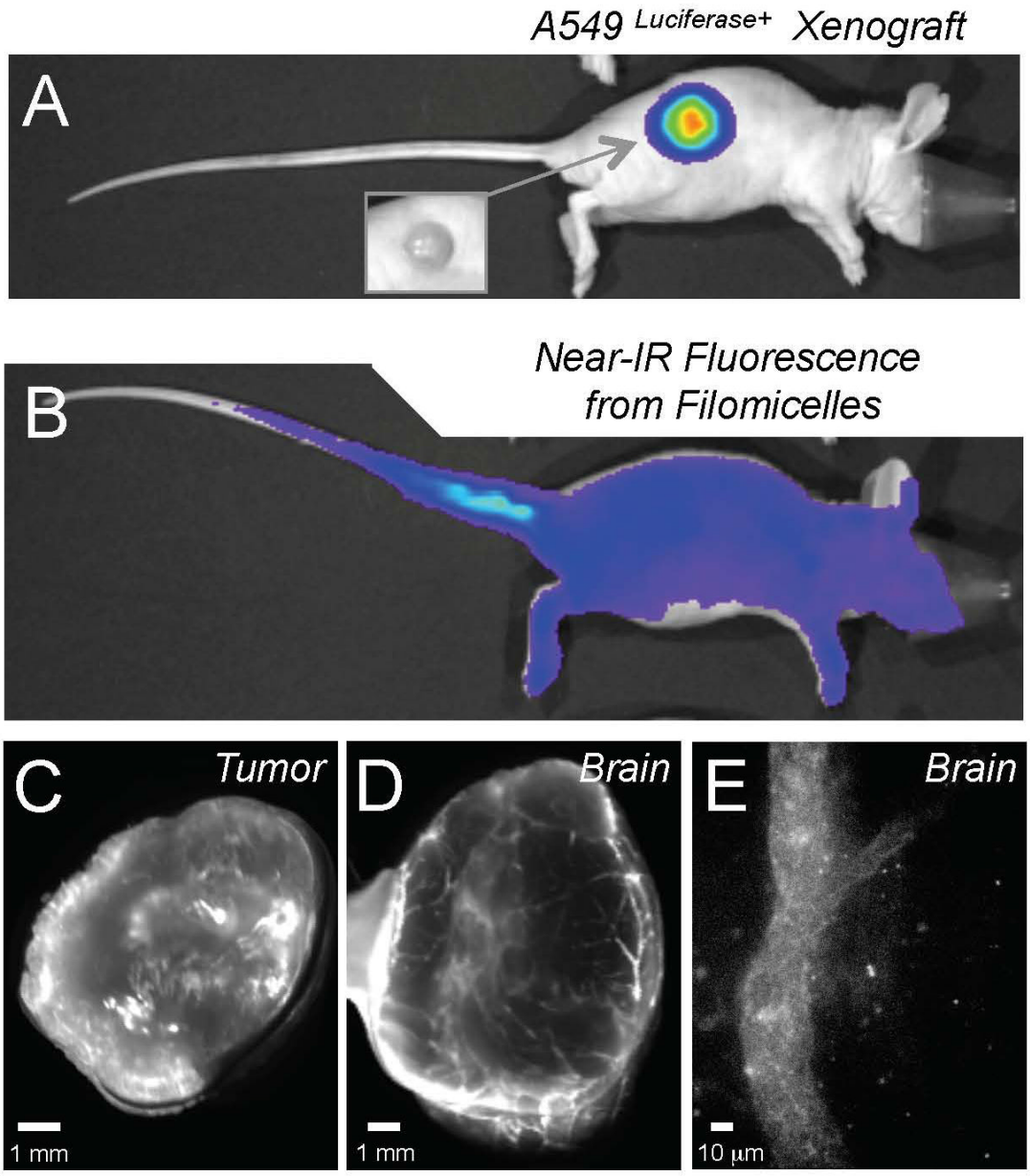

Figure 2. Biodistribution of filomicelles in A549 tumor xenograft mice

(A) Whole body bioluminescent images of luciferase-transfected A549 tumor xenograft mice (Inset: photograph of tumor). (B) NIR fluorescence image of A549 tumor xenograft mouse that shows the diffuse fluorescence of NIRF-labeled filomicelles in circulation. (C) NIRF-labeled filomicelle accumulation in whole excised tumor visualized by low resolution NIR fluorescence imaging. (D) Higher resolution fluorescence image of NIRF-labeled filomicelles in a cryo-section of the excised tumor taken at 60X. (E) Low resolution NIR fluorescence image of brain where the vasculature can be imaged due to NIRF-labeled filomicelles retained in circulation. (F) The NIRF-labeled filomicelles resident in the vasculature also allowed imaging of intact brains at high resolution.

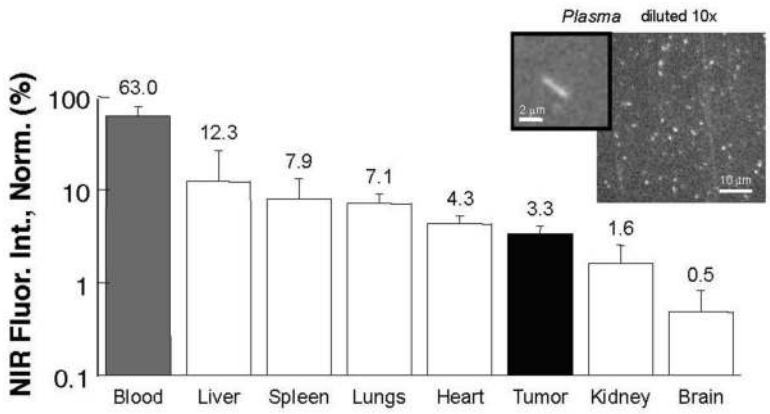

Figure 3. Quantification of the biodistribution of filomicelles in A549 tumor xenograft mice

The fluorescence intensity per organ was normalized for the total intensity per mouse and corrected for tissue thickness by quantifying fluorescence of grossly sectioned tissues. The intensity per organ was also corrected for the estimated fluorescence due to carriers residing in the vasculature of the organ. The value of normalized fluorescence percentage of fluorescence in each. All datapoints show Avg ± S.D. for 3 mice. Inset: Epifluorescence micrographs of 10X diluted plasma 24 h after injection display filomicelles remaining in circulation.

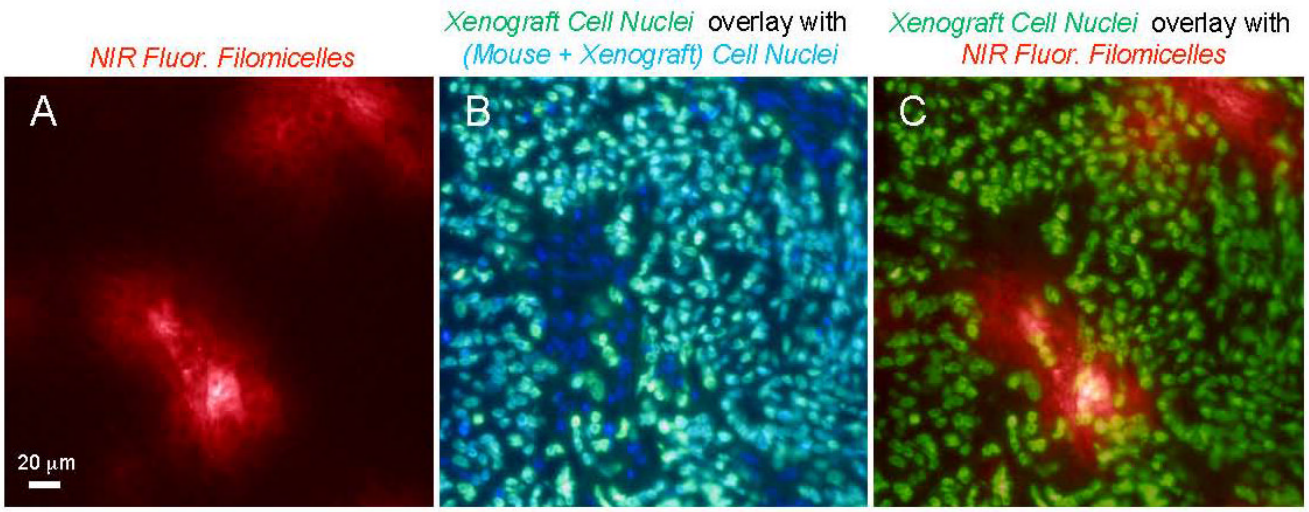

Figure 4. Imaging of DiR-labeled shortened filomicelles in the tumor cryosections

a) Accumulation of NIRF-labeled filomicelles in A549 tumor cryosection. **b)** Fluorescence overlay of immunostaining with human-specific antibody for Lamin A/C (green) and the non-specific Hoescht stain for all nuclei (blue). Nuclei labeled only with blue represent mouse tissue, while colocalized green and blue fluorescence represent human tumor tissue. **c)** Fluorescence overlay of NIRF-labeled filomicelles and Lamin A/C staining shows some colocalization of filomicelles and human tissue (upper right of image), suggesting permeation of filomicelles into the tumor stroma. Fluorescence images of sections were taken after rehydration to remove artifacts resulting from dry or fixed tissue.

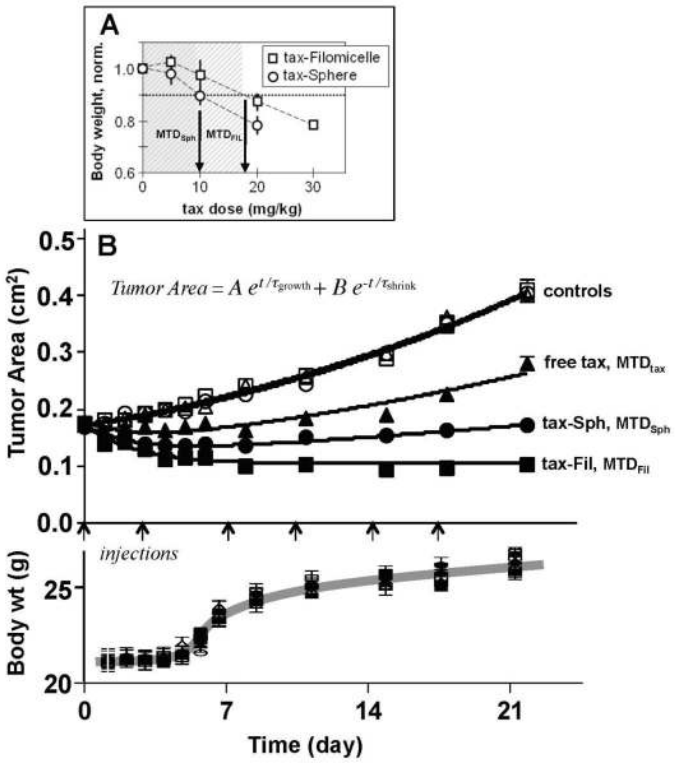

Figure 5. Measurements of Maximum Tolerated Doses and A549 tumor shrinkage after tax administration

(A) MTD determinations with tax in spherical or worm-like morphologies of OCL3 copolymer in nude mice. MTD was defined as the tax dose that caused a loss of body weight ≤10% at 24 h after injection. (B) Upper panel: Tumor inhibition studies over a 3-week period with multiple injections of different treatments including Controls (PBS alone, empty OCL3 spherical or worm-like micelles), free tax in PBS, OCL3 spheres loaded with tax at MTD (~ 8 mg/kg) and OCL3 filomicelles loaded with tax at MTD (~ 16 mg/kg) The tumor growth profile was determined by tumor area, which was monitored 24 h after each injection by measuring two orthogonal dimensions as $[(L_1 \times L_2) / 2]$ (10). The tumor growth-inhibition curves were fit by applying the exponential modeling equation: Tumor Area = $Ae^{t/\tau_{growth}} + Be^{-t/\tau_{shrink}}$, where t is the time (day), A and τ_{growth} are constants of the tumor growth phase, and B and τ_{shrink} are constants of the tax-inhibition phase. The fitted values are listed in Table 2. Lower panel: The body weight changes measured at 24 h after each injection during the 3-week experiment process, showing the mice gained similar in weight for all experimental groups. All datapoints in this figure show (Avg ± S.D.) for 4 mice.

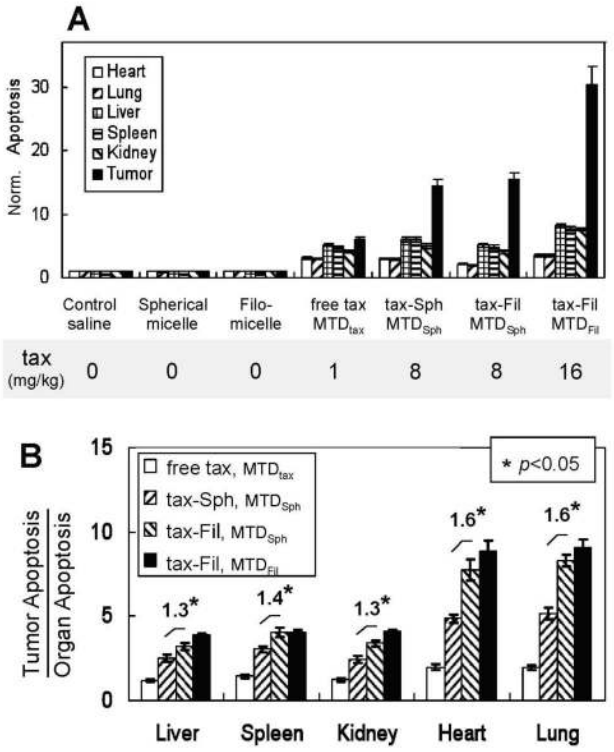

Figure 6. Measurement of cell apoptosis in tumor and non-tumor major organs

Measurements were made after the 22 day multiple injection experiment. (A) Cell apoptosis index measured by ELISA and calculated as: Apoptosis index = Enrichment factor of tax treatment animal groups / Enrichment factor of untreated animal groups; (B) Cell apoptosis index ratio between tumors and other non-tumor organs ($p < 0.05$). All datapoints in this figure show (Avg ± S.D.) for 4 mice.

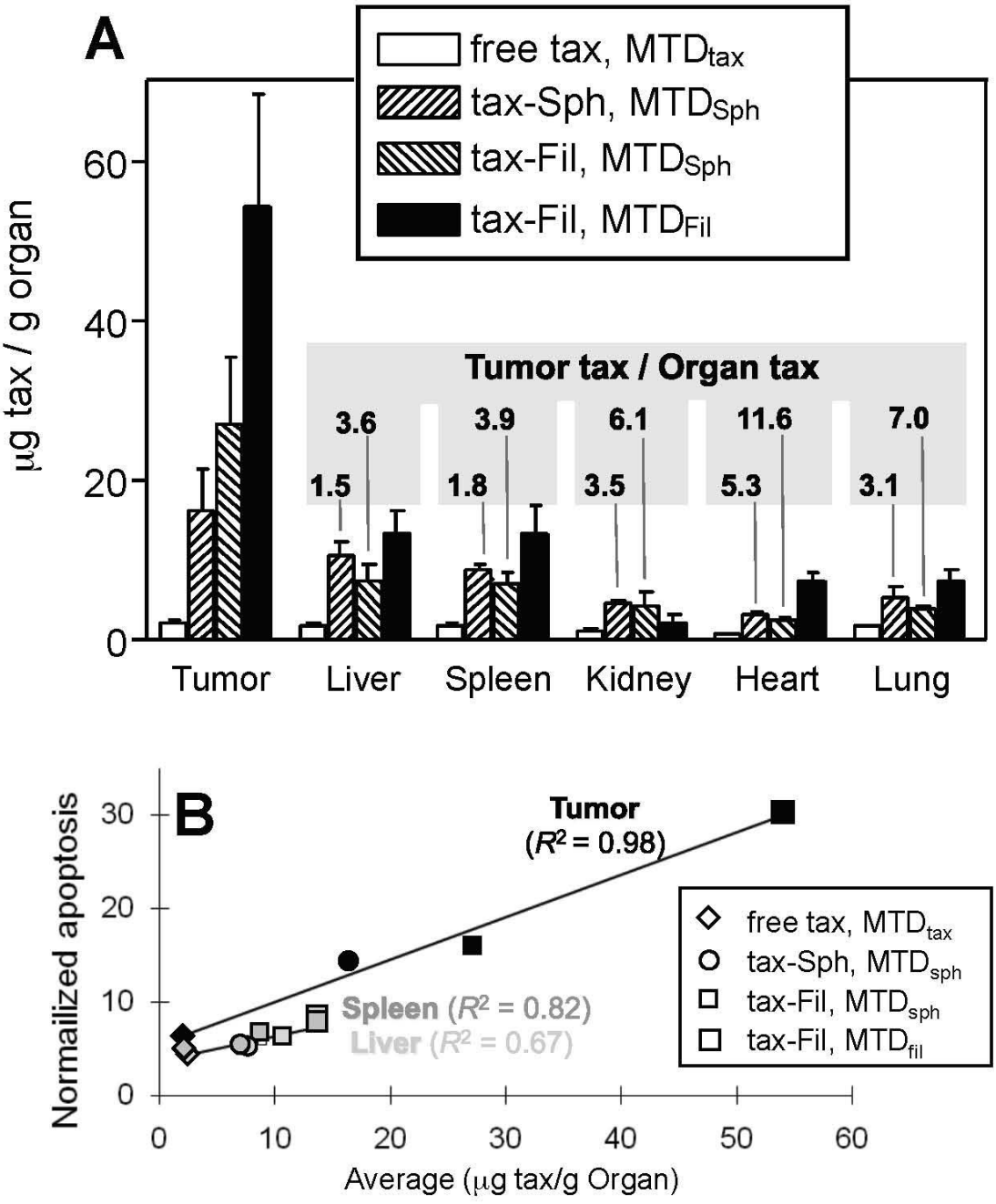

Figure 7. Measurement of tax biodistribution 24 h after single injection

(A) Biodistribution assay of tax in different organs after 24 h of the single I.V. injection, using RP-HPLC method. All datapoints in this figure show (Avg ± S.D.) for 4 mice. (B) Plot of normalized apoptosis vs. average tax distribution for tumor, liver and spleen, fit by y=mx+b, where m (Tumor, Liver, Spleen) = (0.45, 0.24, 0.26).

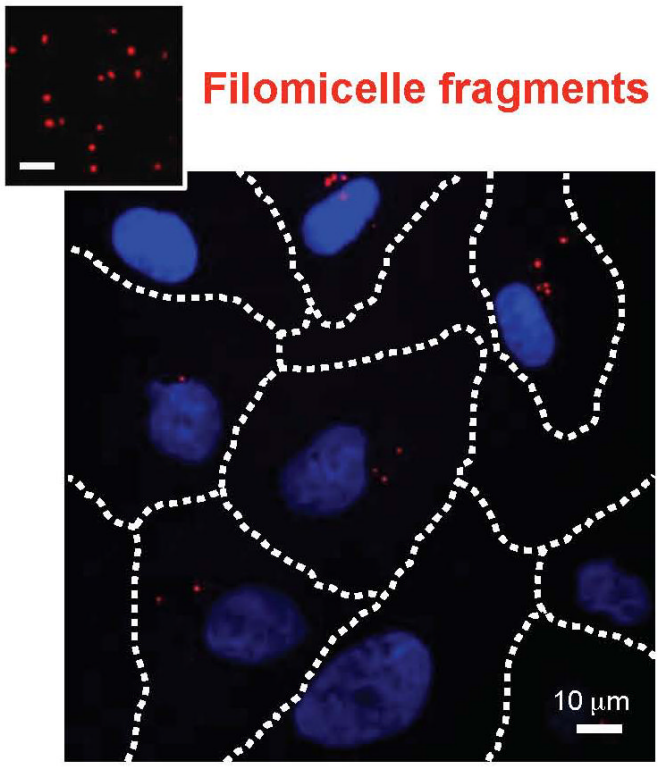

Figure 8. Uptake of OCL micelles by A549 cells *in vitro*

Epifluorescent micrographs of A549 cells after 24 h of incubation with fluorescently-labeled OCL fragmented filomicelles. Cell nuclei were labeled with Hoescht stain without cell fixation, and cells were imaged by DIC to determine cell boundaries. For clarity, cellular boundaries imaged by DIC are represented by dashed lines.

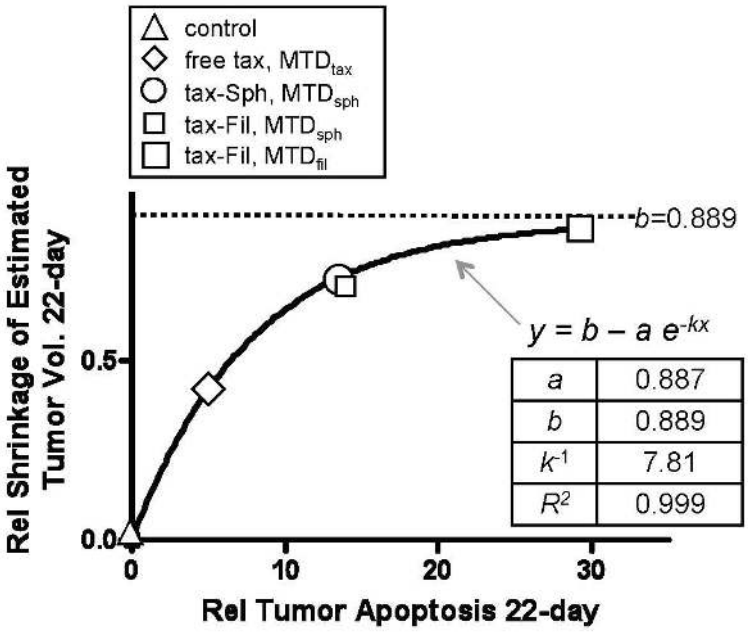

Figure 9. Plot of relative tumor volume shrinkage vs. relative tumor apoptosis at day 22

Relative shrinkage of estimate tumor volume was calculated as: (tumor size in control group — tumor size in treatment group)/(tumor size in control group). Tumor size (cm^3) was estimated from the tumor area (cm^2) in Figure 5, assuming a sphere-shape of tumor. The plot was fit as indicated.

Table 1

Cell apoptosis index ratio between tumor and non-tumor organs in mice, 22 days after multiple intravenous injections of 8 mg/kg tax in OCL3 spherical micelles or OCL3 filomicelles (Avg ± S.D.). Filomicelles consistently cause more cell death in tumors than in other organs

Apoptosis Tumor / Organ	OCL3 Spherical micelles + tax, 8 mg/kg	OCL3 Filomicelles + tax, 8 mg/kg	Change from Spherical micelles to Filomicelles
Tumor / Liver	2.47 ± 0.20	3.19 ± 0.20	+ 29%
Tumor / Kidney	3.07 ± 0.17	4.03 ± 0.26	+ 31%
Tumor / Spleen	2.47 ± 0.21	3.40 ± 0.15	+ 38%
Tumor / Heart	4.85 ± 0.26	7.74 ± 0.65	+ 60%
Tumor / Lung	5.15 ± 0.34	8.31 ± 0.34	+ 61%

Table 2

Fitted constants to model growth and tax-induced shrinkage of the tumor xenografts in Fig. 5B. Tumor growth is slowed to >1 year with Filomicelles compared to a couple of months with Spherical micelles.

	A (cm^2)	τ_{growth} (week)	τ_{shrink} (week)	R^2
Controls	0.168	3.5	∞	0.990
tax	0.108	3.5	1.1	0.947
tax-Sph	0.122	9.4	0.29	0.884
tax-Fil	0.095	59	0.47	0.946